1521-0103/379/3/331–342$35.00
THE JOURNAL OF PHARMACOLOGY AND EXPERIMENTAL THERAPEUTICS

https://doi.org/10.1124/jpet.121.000730
J Pharmacol Exp Ther 379:331–342, December 2021

The Journal of PHARMACOLOGY And Experimental Therapeutics

Pharmacokinetic and Pharmacodynamic Assessment of Hydroxychloroquine in Breast Cancer[S]

Kristen M. Van Eaton and Daniel L. Gustafson

School of Biomedical Engineering (K.M.V.E., D.L.G.), Department of Clinical Sciences (D.L.G.), and Flint Animal Cancer Center (D.L.G.), Colorado State University, Fort Collins, Colorado; and Developmental Therapeutics Program; University of Colorado Cancer Center, Aurora, Colorado (D.L.G.)

Received May 14, 2021; accepted August 26, 2021

ABSTRACT

Hydroxychloroquine (HCQ) is being tested in a number of human clinical trials to determine the role of autophagy in response to standard anticancer therapies. However, HCQ pharmacodynamic (PD) responses are difficult to assess in patients, and preclinical studies in mouse models are equivocal with regard to HCQ exposure and inhibition of autophagy. Here, pharmacokinetic (PK) assessment of HCQ in non–tumor-bearing mice after intraperitoneal dosing established 60 mg/kg as the human equivalent dose of HCQ in mice. Autophagy inhibition, cell proliferation, and cell death were assessed in two-dimensional (2D) cell culture and three-dimensional tumor organoids in breast cancer. Mice challenged with breast cancer xenografts were then treated with 60 mg/kg HCQ via intraperitoneal dosing, and subsequent PK and PD responses were assessed. Although autophagic flux was significantly inhibited in cells irrespective of autophagy-dependence status, autophagy-dependent tumors had decreased cell proliferation and increased cell death at earlier time points compared with autophagy-independent tumors. Overall, this study shows that 2D cell culture, three-dimensional tumor organoids, and in vivo studies produce similar results, and in vitro studies can be used as surrogates to recapitulate in vivo antitumor responses of HCQ.

SIGNIFICANCE STATEMENT

Autophagy-dependent tumors but not autophagy-independent tumors have decreased cell proliferation and increased cell death after single-agent hydroxychloroquine treatment. However, hydroxychloroquine causes decreased autophagic flux regardless of autophagy status, suggesting its clinical efficacy in the context of autophagy inhibition.

Introduction

Macroautophagy ("autophagy") is a normal cellular process in which cell components are taken up by vesicles called autophagosomes that fuse with lysosomes where components are degraded and recycled. Autophagy is induced by metabolic stress and in cells undergoing remodeling or differentiation (De Duve and Wattiaux, 1966; Yang and Klionsky, 2010). It plays important roles in many diseases, including cancer, by enhancing survival and therapy resistance (Duffy et al., 2015). Hydroxychloroquine (HCQ) is a lipophilic weak base that prevents lysosomal acidification by sequestering in lysosomes and raising their pH, in turn blocking the fusion of autophagosomes to lysosomes (Mauthe et al., 2018). HCQ is commonly used as an autophagy inhibitor in cancer clinical trials because it is already Food and Drug Administration–approved, has a low toxicity profile, and is inexpensive (Ruiz-Irastorza et al., 2010; Manic et al., 2014; Thorburn et al., 2014; Cheong, 2015).

HCQ pharmacokinetic (PK) parameters have been well characterized in humans. After oral administration, HCQ is almost completely and rapidly absorbed in the gastrointestinal tract and is about 75% bioavailable (Estes et al., 1987; Carmichael et al., 2003; Lim et al., 2009). Approximately 50% of HCQ is bound to plasma proteins and extensively sequesters in tissue (Tett, 1993; Ducharme and Farinotti, 1996; Lim et al., 2009). It partitions into red blood cells and binds strongly to heme proteins, leading to a high volume of distribution and a prolonged half-life of 40–50 days (Tett, 1993; Ducharme and Farinotti, 1996; Furst, 1996). HCQ is dealkylated in the liver by cytochrome P450 enzymes into active metabolites, including

This work was supported by National Institutes of Health National Cancer Institute [Grant R01CA190170] (Therapeutic Targeting of Autophagy-Dependent Cancer) and by Department of Defense Congressionally Directed Medical Research Programs (CDMRP) Breast Cancer Research Program [Grant BC130103P1] (Identifying and Targeting Autophagy Dependence to Eliminate Metastatic Breast Cancer). This work was also supported by the Drug Development and Discovery Shared Resource of the University of Colorado Cancer Center supported by the Cancer Center Support Grant [Grant P30CA46934] and the Shipley University Chair in Comparative Oncology awarded to D.L. Gustafson.

No author has an actual or perceived conflict of interest with the contents of this article.

dx.doi.org/10.1124/jpet.121.000730.

[S] This article has supplemental material available at jpet.aspetjournals.org.

ABBREVIATIONS: AUC, area under the curve; $AUC_{0\text{-}24}$, area under the curve from time 0 to 24 hours; $AUC_{0\text{-}inf}$, area under the drug concentration versus time curve from time 0 to infinite time; BME, basement membrane extract; 2D, two-dimensional; DHCQ, desethylhyrdoxychloroquine; DMEM, Dulbecco's modified Eagle's medium; EdU, 5-ethynyl-2′-deoxyuridine; HCQ, hydroxychloroquine; HED, human equivalent dose; HRP, horseradish peroxidase; IF, immunofluorescence; PD, pharmacodynamics; PK, pharmacokinetics; TBST, Tris-buffered saline/Tween 80; T_{max}, time to maximal concentration.

desethylhydroxychloroquine (DHCQ) (Ducharme and Farinotti, 1996; Cardoso and Bonato, 2009; Lim et al., 2009). HCQ clearance is divided nearly equally between hepatic and renal mechanisms (Ducharme and Farinotti, 1996).

Although HCQ PK is well described in humans, the pharmacodynamics (PD) associated with HCQ exposure are difficult to assess. There are over 90 cancer clinical trials (ClinicalTrials.gov) that currently investigate or have previously investigated the effects of HCQ alone and in combination with chemo-, immuno-, and radiation therapies. Trials use between 200 and 1200 mg of HCQ daily, but the number of patients with partial or stable responses is variable (Boehrer et al., 2008; Goldberg et al., 2012; Wolpin et al., 2014; Zeh et al., 2020). Further, when assessing patients for LC3-II or p62 accumulation as markers for autophagy inhibition, autophagy inhibition is achievable with HCQ but inconsistent across patient populations (Kimmelman, 2011; Wolpin et al., 2014; Zeh et al., 2020). Monitoring HCQ-driven correlative PD endpoints has not been successful at doses less than the maximum tolerated dose (Mahalingam et al., 2014). Given the large number of clinical trials using HCQ to target cancer, it is important to understand how HCQ exposure modulates cellular responses.

Mice are a widely used preclinical cancer research model system and have been used in numerous autophagy-modulation studies (Amaravadi et al., 2007; Frese and Tuveson, 2007; Komatsu et al., 2007; Duran et al., 2008; Yang et al., 2011). However, many human tumors do not grow in immunodeficient mouse models, which makes it impossible to study certain cancers using this model. For instance, triple-negative breast cancers grow in immunodeficient mouse models, but most luminal estrogen receptor–positive and human epidermal growth factor receptor 2–positive breast xenografts cannot grow (Dobrolecki et al., 2016; Sflomos et al., 2016). However, there are reports of growing these subtypes in three-dimensional cell culture as organoids (Li et al., 2019; Campaner et al., 2020), which is important since organoids have been shown to more closely mimic in vivo responses compared with two-dimensional (2D) cell culture (Bleijs et al., 2019; Yang et al., 2020). In addition, tumor organoids can accurately recapitulate in vivo drug responses, simplify experiments, and save time and money (Sasmita and Wong, 2018; Bleijs et al., 2019; Fan et al., 2019).

Although HCQ is used clinically as an autophagy inhibitor to prevent cancer cell survival and therapy resistance, the efficacy of HCQ is not known in humans and has not been established in mouse models. Here, the human equivalent dose (HED) of HCQ reflected in human clinical trial data was determined in non–tumor-bearing mice, and the response to autophagy inhibition was assessed. Cell proliferation, death, and autophagic flux after HCQ were then evaluated in breast cancer cell lines that are variably dependent on autophagy in vitro. Mice with human breast xenografts were treated with the HED to characterize pharmacodynamic responses in vivo. Understanding HCQ PK and PD allows for comparison with human PK reported in recent trials and subsequently the PD associated with autophagy inhibition.

Materials and Methods

Mouse Treatments. Protocols for animal studies were approved by the Institutional Animal Care and Use Committee at Colorado State University. Six- to 8-week-old non–tumor-bearing female BALB/c mice (Charles River National Cancer Institute, Frederick, MD) were treated with a single intraperitoneal dose of 20, 40, or 80 mg/kg HCQ (Sigma-Aldrich, H0915, Milwaukee, WI). Tissues and whole blood were collected at 3, 6, 12, 24, 48, and 72 hours. For tumor-bearing mice, MDA-MB-231 and MDA-MB-468 breast cancer cell lines were implanted in the third mammary fat pads of 6- to 8-week-old female athymic nude mice (Charles River NCI, Frederick, MD). MCF7 breast cancer cells were implanted in the third mammary fat pads of 6- to 8-week-old ovariectomized female athymic nude mice (Charles River NCI, Wilmington, MA) and supplemented with 0.18 mg 17β-estradiol 60-day slow-release tablets (Innovative Research of America, SE-121, Sarasota, FL). Tumors were grown to between 150 and 400 mm^3 and then treated with a single intraperitoneal dose of 60 mg/kg HCQ or once daily with a 60-mg/kg HCQ intraperitoneal dose for 1 week. Tissues, tumors, and whole blood were collected at 3, 6, 12, 24, 48, and 72 hours after the single dose or 24 hours after the last daily dose.

Drug Measurements. Levels of HCQ and DHCQ in whole blood and tissues were determined via a validated liquid chromatography–tandem mass spectrometry assay as previously described (Barnard et al., 2014). Pharmacokinetic parameters were calculated by noncompartmental analysis using Phoenix WinNonlin (v 8.3.3.33) (Certara, Princeton, NJ).

Western Blot Analysis. Tissues and tumors were flash-frozen in lysis buffer [1% Triton X-100, 150 mM NaCl, 10 mM Tris pH 7.5, 100 mM Na-orthovanadate (Alexis Biochemicals, 400-032-G025, Farmingdale, NY), 34.8 μg/ml phenylmethylsulfonyl fluoride (Fluka Biochemica, 78830, Milwaukee, WI), and 1× protease inhibitor cocktail (Roche, 11836153001, Milwaukee, WI)]. Samples were homogenized for 20 seconds, sonicated with three 3-second bursts on ice, and then centrifuged at 14,000 rpm for 10 minutes at 4°C. Supernatant was collected, and protein concentration was determined using the Pierce BCA Protein Assay Kit (Thermo Scientific, 23225, Rockford, IL). Twenty micrograms of protein were resolved on a 4%–20% SDS-polyacrylamide gel (Bio Rad, 4568095, Hercules, CA) and transferred onto polyvinylidene fluoride membranes (Bio Rad, 1704272, Hercules, CA). Membranes were blocked in 2.5% nonfat dry milk in Tris-buffered saline/Tween 80 (TBST) [10 mM Tris pH 7.5, 100 mM NaCl, and 0.1% Tween 80 (Fisher Chemicals, BP338-500, Fair Lawn, NJ)] for 1 hour at room temperature. Blots were probed with polyclonal anti-LC3B antibody (Novus Biologicals, NB100-2220, Centennial, CO) at 1:1000, monoclonal anti–α-tubulin antibody (Sigma-Aldrich, T5168, St. Louis, MO) at 1:5000, monoclonal anti-p62/SQSTM1 antibody (Novus Biologicals, H00008878-M01, Centennial, CO) at 1:1000, or monoclonal anti–glyceraldehyde-3-phosphate dehydrogenase antibody (Novus Biologicals, NB300-221, Centennial, CO) at 1:1000 in blocking solution overnight at 4°C. Blots were washed three times in TBST and then incubated at room temperature for 1 hour with horseradish peroxidase (HRP)-conjugated secondary antibodies anti—rabbit HRP (Pierce, 31460, Rockford, IL) at 1:2000 or anti–mouse HRP (Pierce, 31430, Rockford, IL) at 1:2000 for p62, 1:5000 for α-tubulin, or 1:10,000 for glyceraldehyde-3-phosphate dehydrogenase in blocking solution. α-Tubulin or total protein was used as housekeeping control. Blots were washed three times with TBST. Immunodetection was carried out using SuperSignal West Dura (Thermo Scientific, 34075, Rockford, IL) and imaged in a ChemiDoc XRS+ (Bio Rad, Hercules, CA) using Image Laboratories version 3.0 software. Densitometry quantification of LC3 and p62 levels was performed by NIH ImageJ software (http://rsb.info.nih.gov/nih-image/) or by Image Laboratories total protein normalization.

Immunofluorescence Analysis. Tumor samples were put into 5% pyridoxal phosphate solution for 24 hours at 4°C and then placed in 30% sucrose solution for 24 hours at 4°C. Samples were fixed in 4% paraformaldehyde, placed in optimal cutting temperature compound, and cryosectioned at 5 μm. Sample slides were rehydrated in PBS plus 0.05% Tween 20 then washed with 0.1M glycine/PBS to reduce tissue autofluorescence. Nonspecific binding was blocked with 5% donkey serum in immunofluorescence (IF) buffer (0.2% Triton X-100, 0.1% bovine serum albumin, 0.05% Tween 20, PBS) for 30 minutes at room temperature. Sections were probed for primary anti-Ki67 (Cell Signaling Technology, 9027, Danvers, MA) diluted 1:400, primary anti–cleaved caspase-3 (Cell Signaling Technology, 9664, Danvers,

MA) diluted 1:200, or rabbit IgG isotype control (Cell Signaling Technology, 3900, Danvers, MA) diluted to the same concentration as other primary antibodies in IF buffer for 1 hour at room temperature. Slides were washed three times in PBS plus 0.05% Tween 20, incubated with Cy3 secondary antibody (Jackson ImmunoResearch, 711-165-152 lot 142318, West Grove, PA), and diluted 1:200 in IF buffer for 30 minutes at room temperature. Three washes were performed, and then slides were counterstained with filtered 4′,6-diamidino-2-phenylindole working solution (Thermo Scientific, 62248, Rockford, IL) diluted 1:500 in PBS for 15 minutes at room temperature. Slides were cover-slipped with ProLong Diamond Antifade Mountant (Invitrogen, P36961, Eugene, OR) and imaged using an Olympus IX83 confocal microscope and Hamamatsu digital camera.

Cell Culture. Cell lines were validated mycoplasma-free and maintained at 37°C and 5% CO_2 in Dulbecco's modified Eagle's medium (DMEM) (Corning, 10-017-CV, Manassas, VA) buffered with 10 mM HEPES (Fisher Scientific, BP-299-100, Denver, CO) and supplemented with 10% FBS (Peak Serum, PS-FB3, Wellington, CO), 1% penicillin-streptomycin (Corning, 30-002-CI, Manassas, VA), and 1% sodium pyruvate (Corning, 25-000-CI, Manassas, VA). MCF7 media were also supplemented with 10 μg/ml insulin (Fisher Scientific, 12585014, Grand Island, NY). Cells were used for no more than 20 passages.

Organoid Culture. To form organoids, cells were grown on Cultrex 3D Culture Matrix Reduced Growth Factor Basement Membrane Extract (BME) (R&D Systems, 344501001, Minneapolis, MN). Briefly, 100 μl/cm^2 BME was plated and allowed to solidify at 37°C for a minimum of 30 minutes before plating cells. Cells were grown for 2 days on BME prior to addition of drug.

Drug Sensitivity, Cell Death, and Autophagic Flux Live-Cell Imaging Assays. For 2D HCQ drug sensitivity, cell death, and autophagic flux assays, 3000 cells were plated per well in a 96-well plate a few hours before drugging. NucLight red–labeled cells were used for drug sensitivity and cell death assays, and cells transduced with LC3-mCherry-GFP were used for autophagic flux assays. For HCQ sensitivity assays, cells were treated with HCQ concentrations ranging from 0 to 40 μM HCQ. For the apoptosis assays, cells were plated in buffered minimum Eagle's medium (Corning, 10-010-CV, Manassas, VA) 5 hours before drugging with 10 μM HCQ (equal dosing) and either 8 μM (MDA-MB-231 and MDA-MB-468) or 15 μM (MCF7) HCQ (equal toxicity) combined with 5 μM caspase 3/7 green fluorescent dye (Essen BioScience, 4440, Ann Arbor, MI). For cytotoxicity assays, cells were plated in buffered minimum Eagle's medium 5 hours before drugging with 10 μM HCQ and either 8 μM (MDA-MB-231 and MDA-MB-468) or 15 μM (MCF7) HCQ combined with 100 nM YOYO green fluorescent dye (Invitrogen, Y3601, Eugene, OR). For autophagic flux assays, cells were plated in buffered DMEM 5 hours before drugging with 10 μM HCQ and either 8 μM (MDA-MB-231 and MDA-MB-468) or 15 μM (MCF7) HCQ. Plates were imaged once every 24 hours on an IncuCyte Zoom (Essen BioScience, Ann Arbor, MI). All organoid cultures were performed the same way except 5000 cells/well were plated on 100 μl/cm^2 BME 2 days prior to drugging.

Cell Cycle Analysis. Three hundred thousand cells per well were plated in 6-well plates the day before drugging with HCQ. Cells grew for 48 hours after drugging and then were trypsinized, spun down, washed once with PBS, fixed with 70% ethanol, and stored at −20°C for up to 2 weeks. Cells were stained with FxCycle PI/RNase (Life Technologies, F10797, Carlsbad, CA) at a concentration of 2 million cells/ml then analyzed on a Gallios flow cytometer (Beckman Coulter). Flow results were analyzed via FlowJo.

Cell Proliferation via 5-Ethynyl-2′-deoxyuridine Staining. For 2D cell culture experiments, 750,000 cells/plate were plated in 60-mm dishes the day before drugging with HCQ. Once drugged with HCQ, cells grew for 48 hours. One (MCF7 and MDA-MB-231) or 2 hours (MDA-MB-468) before the 48-hour time point, cells were treated with 10 μM 5-ethynyl-2′-deoxyuridine (EdU). Cells were trypsinized, spun down, washed once with cold PBS, and then fixed in ice-cold 70% ethanol. Fixed cells were stored at 4°C for a minimum of 2 days. Cells were rehydrated in PBS for 1 hour and then stained using the Click-iT EdU flow cytometry Alexa Fluor 647 kit (Invitrogen, C10424, Eugene, OR) by permeabilizing and staining cells. Cells were washed an extra time with PBS just before being put in a final concentration of 1 million cells/ml in PBS. One hundred micrograms per milliliter RNase A (Thermo Scientific, FEREN0531, Carlsbad, CA) and 1 μl of a 1:4 dilution from stock Sytox Blue (Thermo Scientific, S34857, Eugene, OR) were added per 1 million cells. Cells were incubated overnight before flow on a Gallios flow cytometer.

For tumor organoid experiments, 100 μl/cm^2 BME was plated, and then 30 minutes later, 750,000 cells were plated. Tumor organoids were allowed to establish for 2 days before treatment with HCQ. Once drugged with HCQ, cells grew for 48 hours. Four hours before the 48-hour time point, cells were treated with 10 μM EdU. Cells were isolated from BME using cell harvesting buffer (R&D Systems, 3448020CH, Minneapolis, MN) protocol. Briefly, cells were washed three times with PBS, cell harvesting buffer was added to the plate on ice, and cells were pipetted up and down, moved to a 15-ml conical, topped with cell harvesting buffer, and shaken on a plate shaker at 650 rpm for 30 minutes at 4°C. Conical tubes were centrifuged, supernatant was removed, and cells were washed once more with cell harvesting buffer. To break up organoids, cells were incubated with trypsin at room temperature for 10 minutes and then fixed with 4% paraformaldehyde for 15 minutes. Cells were permeabilized and stained after the Click-iT EdU flow cytometry Alexa Fluor 647. Cells were washed an extra time with PBS and then incubated with 100 μg/ml RNase A and 1 μl of a 1:4 dilution from stock Sytox Blue per 1 million cells for a minimum of 30 minutes before being analyzed on a Gallios flow cytometer. All results were analyzed via FlowJo.

Autophagic Flux Flow Cytometry. Cells transduced with an LC3-mCherry-GFP reporter were used. Cells were plated at 325,000 cells/well in a 6-well plate for 24 hours, 200,000 cells/dish in a 60-mm dish for 96 hours, or 50,000 (MDA-MB-231) or 100,000 (MCF7, MDA-MB-468) cells/plate for 144 hours in a 60-mm dish; allowed a day to attach and grow; and then drugged with HCQ. For use in flow cytometry analysis, control cells were treated with 10 nM bafilomycin A1 (Fisher Scientific, AAJ67193XF, Ward Hill, MA) 24 hours prior to the endpoint to completely inhibit autophagy. Cells were trypsinized, washed once with cold PBS, and resuspended in PBS, keeping cold and on ice. Samples were flowed on an Aurora 4 laser (Cytek Biosciences, Fremont, CA) flow cytometer, and then data were analyzed via FlowJo. To determine the percentage of cells using autophagy, the bafilomycin-treated control cells were gated so that 5%–10% of cells were positive in an angled, diagonal area to the upper left of the events on an mCherry versus GFP plot. This gate was pasted directly onto all other samples for the same cell line from the same replicate.

Live/Dead Staining. Seven hundred thousand cells per plate for 48 hours, 200,000 cells/plate for 96 hours, or 50,000 cells/plate for 144 hours were plated in 60-mm dishes the day before drugging with HCQ. Cells were grown for given time frame and then trypsinized, spun down, and washed once with cold PBS. Cells were resuspended in PBS at a concentration of 1 million cells/ml, and then 1 μl of a 1:4 dilution from stock Sytox Blue was added. Cells were incubated for 15 minutes at room temperature, then kept on ice until ready to flow, and analyzed on a Gallios flow cytometer as soon as possible. Results were analyzed via FlowJo.

Statistical Analysis. Statistical analysis was performed using Graphpad Prism. Two-way ANOVA using multiple comparisons with Dunnett correction between controls and drug-treated cells at each time point or unpaired two-tailed t tests between controls and HCQ-treated mice were used to determine statistical significance with $*P \leq 0.05$, $**P \leq 0.01$, $***P \leq 0.001$, or $****P \leq 0.0001$. All error bars are standard deviation.

Results

HCQ Exposure Is Dose-Dependent In Vivo. HCQ and DHCQ levels were measured in whole blood, liver, gut, kidney,

and brain after a single intraperitoneal dose of 20, 40, or 80 mg/kg HCQ (Fig. 1A; Supplemental Fig. 1). Drug levels were dose-dependent, and concentrations of HCQ and DHCQ decreased over time. Highest concentrations were observed in the liver. In whole blood, there were still detectable levels of HCQ and DHCQ at 72 hours after all doses. HCQ levels were undetectable in the liver after 24 hours, but DHCQ levels were detectable at relevant concentrations up to 72 hours. Concentrations of HCQ and DHCQ in the gut were similar over the entire 72 hours, with slightly more DHCQ than HCQ present at all doses 24 hours and later. Kidney drug levels were similar to those in the gut and showed the same trends with higher DHCQ levels after 12 hours. HCQ can cross the blood-brain barrier (Amaravadi et al., 2011) and therefore can be detected in the brain. The concentrations of HCQ and DHCQ in the brain were approximately 10-fold less than whole blood, liver, kidney, and gut, which suggests that HCQ and DHCQ enter the central nervous system to a lesser degree than other tissues.

HCQ PK parameters (Supplemental Table 1; Table 1) show that C_{max} in whole blood, liver, gut, kidney, and brain increased in a dose-dependent manner. Time to maximal concentration (T_{max}) occurred at 3 hours in whole blood, liver, gut, kidney, and brain at all doses except for brain at 80 mg/kg, in which T_{max} occurred at 6 hours. Half-lives for whole blood, liver, gut, kidney, and brain were approximately 14.5, 3.5, 17.5, 15, and 48 hours, respectively, regardless of dose. The area under the drug concentration versus time curve from time 0 to infinite time ($AUC_{0\text{-}inf}$) increased as dose increased in all tissues, which shows that exposure of HCQ is dose-dependent. DHCQ PK parameters in whole blood (Supplemental Table 2) and tissues (Supplemental Table 3) had similar trends as HCQ. C_{max} and $AUC_{0\text{-}inf}$ increased in a dose-dependent manner. DHCQ T_{max} occurred mostly between 5 and 9 hours in all tissue. DHCQ half-lives are all slightly longer than HCQ for all tissues except the brain, wherein DHCQ is more rapidly eliminated. HCQ and DHCQ clearance is not constant between 20 and 80 mg/kg. Given that $AUC_{0\text{-}inf}$ is not dose-proportional from 40 to 80 mg/kg and clearance is concurrently increasing, this signifies nonlinear PK with less drug in the blood at higher HCQ concentrations. A potential explanation is an increase in cellular lysosomal volume associated with lysosomal biogenesis triggered by HCQ (Collins et al., 2021), leading to an increase in tissue uptake and subsequent lower blood levels. This explanation is supported by the relationship between dose and area under the curve (AUC) for blood versus tissues in which whole blood shows a 1.80- and 3.07-fold increase in AUC when doses are increased 2- and 4-fold, whereas tissues (brain, gut, kidney, and liver) all show fold increases greater than 2 and 4 with averages of 2.47 ± 0.28 and 4.78 ± 0.71. Thus, although dose and exposure (AUC) are related for all tissues analyzed, tissue accumulation increases greater than the fold dose increase, whereas blood increases at a rate lower than the fold increase.

To determine equivalent dose exposure for HCQ in mice compared with humans, area under drug concentration versus time curves from both mice and humans were directly compared since these AUCs represent exposure in each species. The HED of steady-state HCQ concentration was calculated by using the average human patient AUC over a 24-hour dosing time period estimated at steady state in humans given an oral 600-mg dose (Rosenfeld et al., 2014) and comparing this to the area under the curve from time 0 to 24 hours ($AUC_{0\text{-}24}$) corrected with an accumulation factor in mice found in this study. A comparison of the predicted trough level (24 hours) at 60 mg/kg in the Balb/c non–tumor-bearing mice at steady state versus the measured steady-state levels in tumor-bearing mice at 24 hours showed a predicted value of 227 ng/ml and measured values at 288 ± 75 ng/ml. The HED in mice is 60 mg/kg in whole blood with a standard deviation of 20 mg/kg (Fig. 1B), suggesting most doses used for in vivo mouse studies are within the limits of exposure achievable in humans. The $AUC_{0\text{-}24}$ that was measured in the tumor-bearing mice at 60 mg/kg (Table 1) corrected for accumulation at steady state (1.47-fold) gives a calculated exposure of 32.8 μg × h/ml, which is consistent with the exposure range shown in Fig. 1B.

Autophagy Inhibition Is Variable in Tissues. Pharmacodynamic response was assessed by Western blot analysis of LC3 and p62 in the liver, kidney, gut, and brain at various time points (Fig. 1C; Supplemental Fig. 2). Autophagy inhibition in the liver was observed at later time points, most noticeably at 48 hours based on the LC3-II/tubulin ratio. Since liver autophagy was inhibited most at later time points, only 24-, 48-, and 72-hour time points were assessed in the gut, kidney, and brain. The gut and the kidney showed no autophagy inhibition by either LC3 or p62 levels. Brain autophagy inhibition was evident in a few mice at 24 and 48 hours but was not dose-related. There was no difference in p62 expression in controls compared with HCQ-treated mice in the liver or kidney. Effects of HCQ and DHCQ on LC3-II expression over time measured by Western blot in the liver demonstrate counterclockwise hysteresis, showing that it takes time for enough HCQ and DHCQ levels to build up before an effect is observed (Fig. 1D; Supplemental Fig. 3). There is not much difference between the curves when comparing LC3-II levels to either whole-blood or liver HCQ concentrations, indicating that HCQ whole-blood concentrations can be used as a surrogate for autophagy effects. Furthermore, DHCQ has a similar effect as HCQ on LC3-II levels. When HCQ and DHCQ concentrations are added together to determine total active drug, the hysteresis curves are still counterclockwise and similar to HCQ or DHCQ alone, indicating that although DHCQ is active, it does not significantly change how quickly autophagy is affected and also requires a buildup to achieve an effect.

HCQ Exhibits Antiproliferative Effects and Decreases Autophagic Flux but Does Not Induce Significant Cell Death in In Vitro 2D Culture. In vitro two-dimensional cell culture experiments were performed to validate standard cell culture methods as a sufficient pharmacodynamic model comparable to in vivo results and to assess how HCQ is affecting cell growth, death, and long-term autophagy in breast cancer. To investigate differences in HCQ uptake, response between breast cancers with different sensitivities to autophagy inhibition determined via shRNA knockdowns and responses to chloroquine in vitro and when grown as tumor xenografts (Maycotte et al., 2014), MDA-MB-468 (triple negative basal), MDA-MB-231 (triple negative claudin-low), and MCF7 (luminal) cells, listed from most autophagy-sensitive to least autophagy-sensitive, were treated with increasing doses of HCQ in buffered DMEM for up to 120 hours. Cells are more affected by lower doses of HCQ at later time points (Fig. 2A). The ED_{50} at which half of cells were affected at 96 hours was calculated. As expected, autophagy-independent

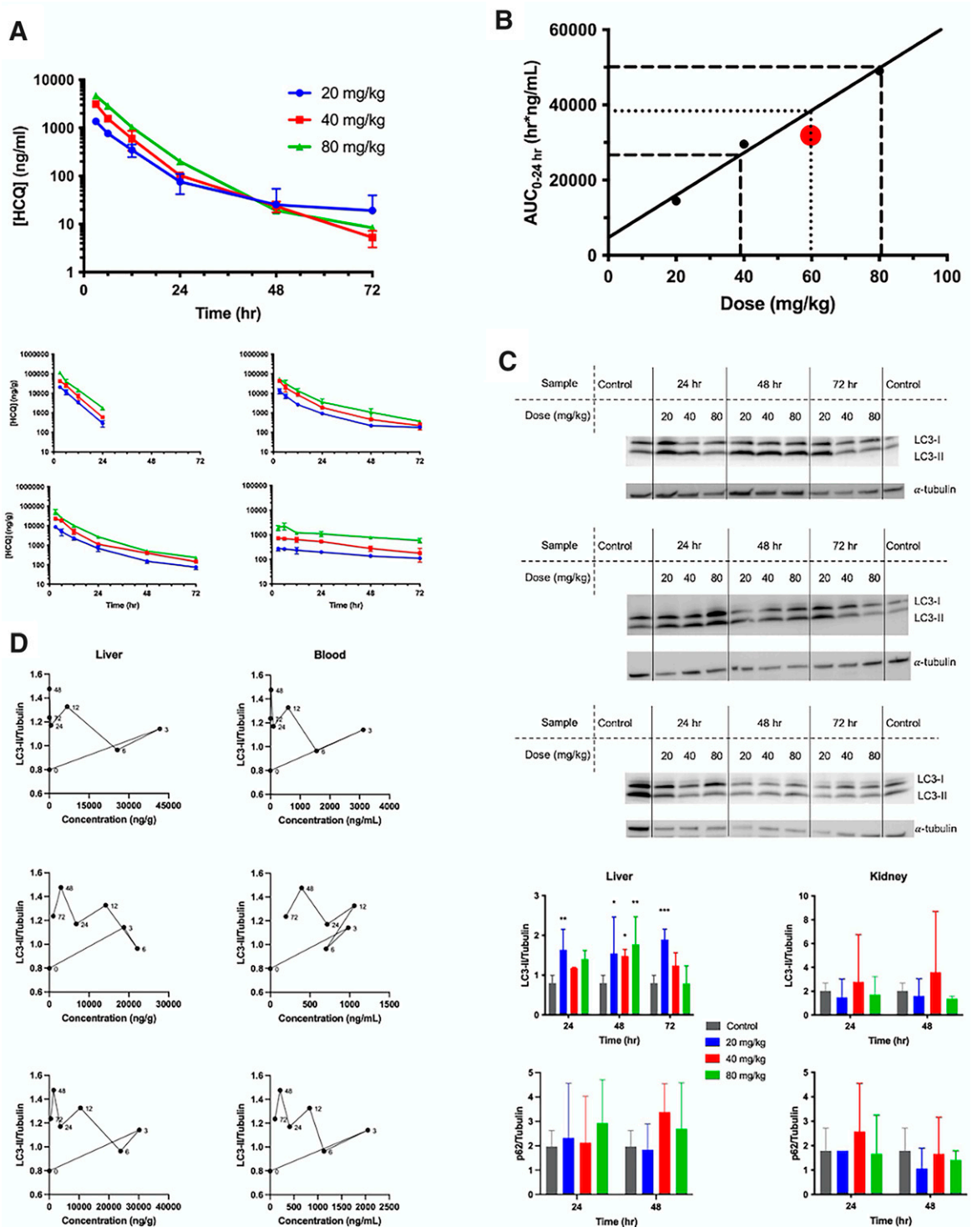

Fig. 1. HCQ PK and associated PD in non–tumor-bearing mice. (A) Exposure of HCQ and DHCQ in whole blood, liver, gut, kidney, and brain. (B) Clinical trial human HCQ AUC data (Rosenfeld et al., 2014) were compared with mouse AUC data to find the human equivalent dose in mice. The dotted line represents the mean human HCQ AUC, and dashed lines represent human HCQ AUC standard deviation. The red dot represents the $AUC_{0\text{-}24}$ estimated at steady state from the tumor-bearing mouse PK study dosed at 60 mg/kg. (C) LC3 Western blots for the liver 24, 48, and 72 hours after HCQ in three mice. LC3 and p62 Western blot quantification for liver and kidney from Western blots shown in Supplemental Fig. 2. (D) Hysteresis curves showing how LC3-II levels as measured in the liver are affected by HCQ and DHCQ concentrations in the liver or whole blood after 40-mg/kg dose of HCQ. Numbers on the curves correspond to the time points. $N = 3$ mice per group. $^{*}P \leq 0.05$, $^{**}P \leq 0.01$, $^{***}P \leq 0.001$, and $^{****}P \leq 0.0001$.

MCF7 had the highest ED_{50} of 14.6 ± 2.9 μM, whereas autophagy-dependent MDA-MB-231 and MDA-MB-468 ED_{50} values were lower at 7.8 ± 3.9 μM and 7.9 ± 2.6 μM, respectively (Fig. 2A).

Since patients with cancer are generally treated with 200–400 mg HCQ, the maximal concentration of HCQ achievable in patients is equivalent to 10 and 20 μM in vitro based on dosing an average-size patient. Therefore, cells were

TABLE 1
Pharmacokinetic parameters of HCQ from whole blood in non–tumor-bearing and tumor-bearing mice after a single intraperitoneal dose

		Dose			
		Non–Tumor-Bearing Balb/c Mice			MDA-MB-231 Tumor–Bearing Nude Mice
PK Parameter	Units	20 mg/kg	40 mg/kg	80 mg/kg	60 mg/kg
C_{max}	μg/ml	1.36	3.12	4.66	3.56
T_{max}	h	3	3	3	3
$t_{1/2}\lambda$	h	24.1	11.2	13.4	10.2
$AUC_{0\text{-inf}}$	μg•h/ml	13.55	24.26	40.39	29.66
$AUC_{0\text{-}24h}$	μg•h/ml	9.09	17.64	30.31	22.34
*CL	l/h/kg	1.49	1.65	1.98	2.02
MRT	h	16.2	9.0	8.8	8.9
*V_Dz	l/kg	51.6	26.6	30.0	39.0

CL, clearance; MRT, mean resistance time; t1/2λ, terminal half-life; V_Dz, apparent volume of distribution.
*CL and V_Dz calculations represent values that are not dose-corrected for the bioavailability, and total dose was used in the calculation.

treated with either 10 μM (equal dosing) or their ED_{50} value (equal toxicity, 8 μM for MDA-MB-231 and MDA-MB-468 and 15 μM for MCF7) for the following experiments. Equal dosing means cells were treated with the same concentration of HCQ, and equal toxicity means cells were treated at the HCQ concentration in which half of the cells were affected. To determine whether the cells were dying via apoptosis, cells were treated with HCQ for 144 hours with a caspase 3/7 fluorescent dye and monitored in a live-cell imaging system. There were no differences in caspase 3/7 signal between control and HCQ-treated cells in any cell line (Fig. 2B; Supplemental Fig. 6A), indicating that either cell growth is inhibited or that cells are dying by another cell death pathway. To assess whether HCQ causes death in a caspase 3/7–independent manner, cell death was measured in a live-cell imaging system using the cytotoxicity agent YOYO, a fluorescent dye that is cell membrane impermeable and binds free DNA in solution as an indicator of cell death (Fig. 2C; Supplemental Fig. 6B). No difference between control and HCQ-treated cell death was detected. However, when cells were stained with a live/dead stain and analyzed via flow cytometry after 48, 96, or 144 hours of HCQ treatment, modest cell death that was time- and dose-dependent was observed in the autophagy-dependent cells (Supplemental Fig. 4A). Overall, this indicates that cell death is not the major cellular pharmacodynamic response to HCQ in 2D culture.

To discern whether cells were growth-inhibited, cell cycle assays were performed after HCQ dosing for 48 hours. Cell cycle analysis showed that when HCQ concentration is high enough, an increase in G1 and a decrease in G2/M and S are observed (Supplemental Fig. 4B). MCF7 cells treated with 10 μM (less than the ED_{50}) have similar percentages of cells to control in these phases compared with 15 μM. In contrast, MDA-MB-231 and MDA-MB-468 cells experienced a decrease in G2/M and an increase in G0/G1 at all HCQ doses used (their ED_{50} and higher). These results were further supported by cell cycle analysis via EdU incorporation. After HCQ treatment of 48 hours, there were more MDA-MB-231 and MDA-MB-468 cells in G1 and fewer cells in S and G2/M phases of the cell cycle when treated with both HCQ concentrations, but MCF7 cells treated with 10 μM were not as different from their control counterparts as the MCF7 cells treated with 15 μM were (Fig. 2D). Changes in cell cycle were most enhanced in MDA-MB-468, which indicates that HCQ more greatly affects cells that are inherently autophagy-dependent.

Autophagic flux after HCQ treatment was assessed by flow cytometry using cells transduced with an LC3-mCherry-GFP reporter. This reporter works by tagging autophagosomes. GFP gets quenched in acidic environments. Therefore, when an autophagosome fuses with a lysosome, GFP signal decreases and indicates autophagic flux is occurring. Autophagy was inhibited significantly in the MCF7 cells after as little as 24 hours, but autophagy inhibition was not significant in the MDA-MB-231 and MDA-MB-468 until 144 or 96 hours, respectively (Fig. 2E; Supplemental Fig. 6C). Results were similar using a live-cell imaging system (Supplemental Figs. 4C and 6D). This indicates that HCQ has prolonged PD affects that may not be observed at short time points.

HCQ Induces Cell Death and Decreases Autophagic Flux in Tumor Organoids. Cells were grown on a basement membrane matrix to obtain three-dimensional tumor organoids to better recapitulate in vivo tumors. Caspase 3/7–dependent cell death was assessed by live-cell imaging in the IncuCyte. There was significant caspase 3/7 cell death in MCF7 at 96 hours, but by 144 hours, the difference between control and HCQ-treated organoids was no longer significant. No significant caspase 3/7 cell death was observed in MDA-MB-468 organoids, but there was caspase 3/7–dependent cell death in MDA-MB-231 organoids treated with HCQ 96 hours and later (Fig. 3A; Supplemental Fig. 7A). Cytotoxicity measured by YOYO staining showed significant cell death in MDA-MB-231 and MDA-MB-468 organoids at time points as early as 72 hours after HCQ treatment but not significantly in the MCF7 organoids at equal dosing until 120 hours (Fig. 3B; Supplemental Fig. 7B), which indicates that HCQ causes more cell death in autophagy-dependent tumors than autophagy-independent tumors.

Cell cycle analysis was assessed in tumor organoids via EdU incorporation (Fig. 3C). Results were similar to 2D culture; there was no difference in HCQ-treated MCF7 cells compared with controls, but MDA-MB-231 and MDA-MB-468 cells both had significantly fewer cells in S phase at both HCQ concentrations used. Consistent with the 2D results, MDA-MB-468 cells also had a significant increase in G1 cells after HCQ treatment.

To assess autophagic flux, organoids transduced with an LC3-mCherry-GFP construct were imaged in the IncuCyte over 6 days. Similar to the 2D cell culture results, autophagy was inhibited significantly between control- and HCQ-treated organoids at later time points (Fig. 3D; Supplemental Fig.

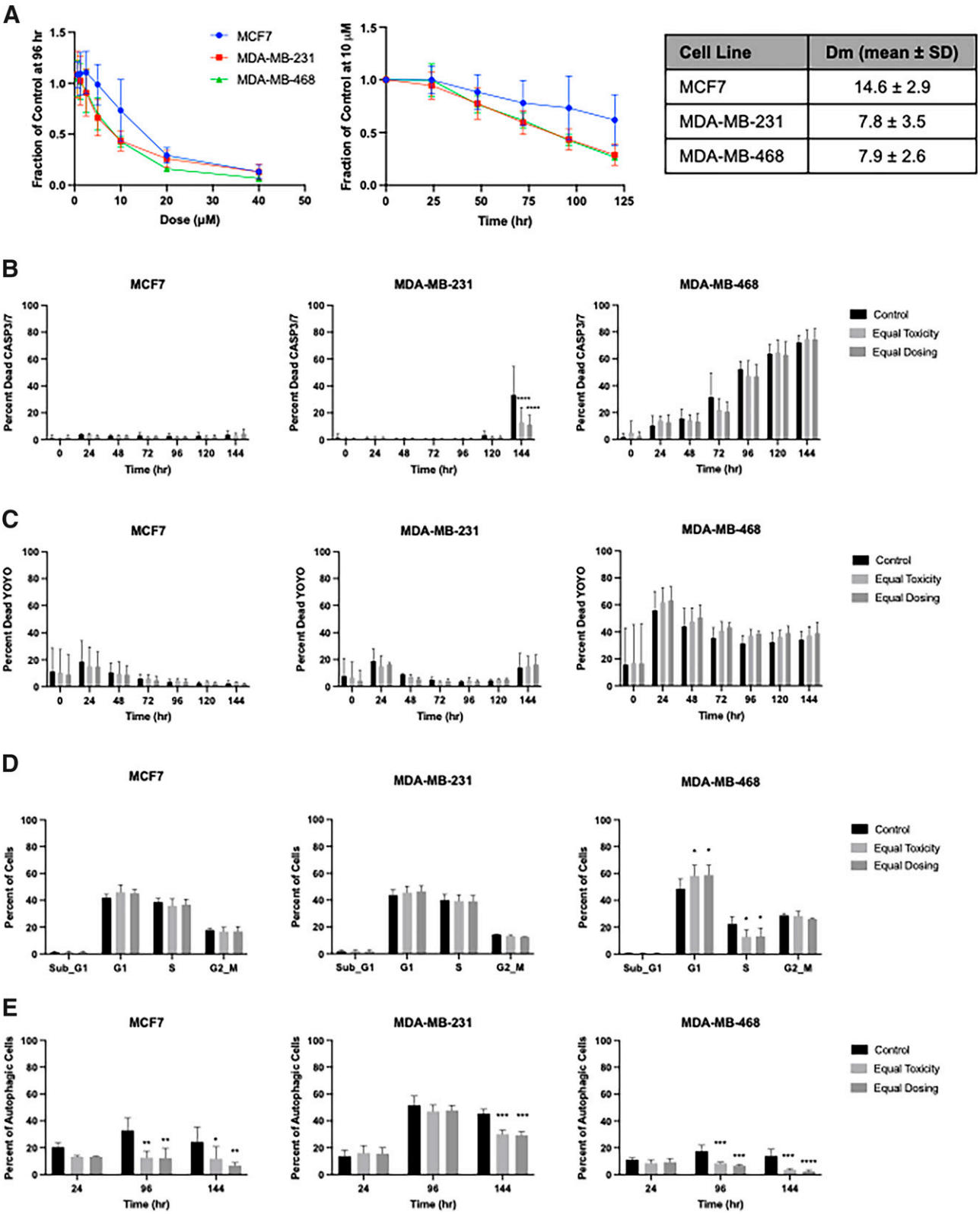

Cell Line	Dm (mean ± SD)
MCF7	14.6 ± 2.9
MDA-MB-231	7.8 ± 3.5
MDA-MB-468	7.9 ± 2.6

Fig. 2. Cell death, cell cycle, and autophagic flux after HCQ treatment in 2D cell culture. (A) HCQ screen in breast cancer lines in buffered media from 0.625 to 40 μM HCQ. The ED_{50} at which half of the cells were affected was calculated at 96 hours. (B) Caspase 3/7 assays on HCQ-treated cells using the live-cell imaging IncuCyte Zoom system. (C) Cell death via YOYO staining using the IncuCyte Zoom. (D) Cell cycle analysis via EdU incorporation of HCQ-treated cells for 48 hours. (E) Autophagic flux was assessed using cells transduced with an LC3-mCherry-GFP reporter and reporting the percentage of cells using autophagy. Equal toxicity doses were 8 μM for MDA-MB-231 and MDA-MB-468 and 15 μM for MCF7. Equal dosing was 10 μM HCQ. $N = 3$ or more biologic replicates of three technical replicates each. Significance indicated is compared with control. $^{*}P \leq 0.05$, $^{**}P \leq 0.01$, $^{***}P \leq 0.001$, and $^{****}P \leq 0.0001$. Dm, median effective dose.

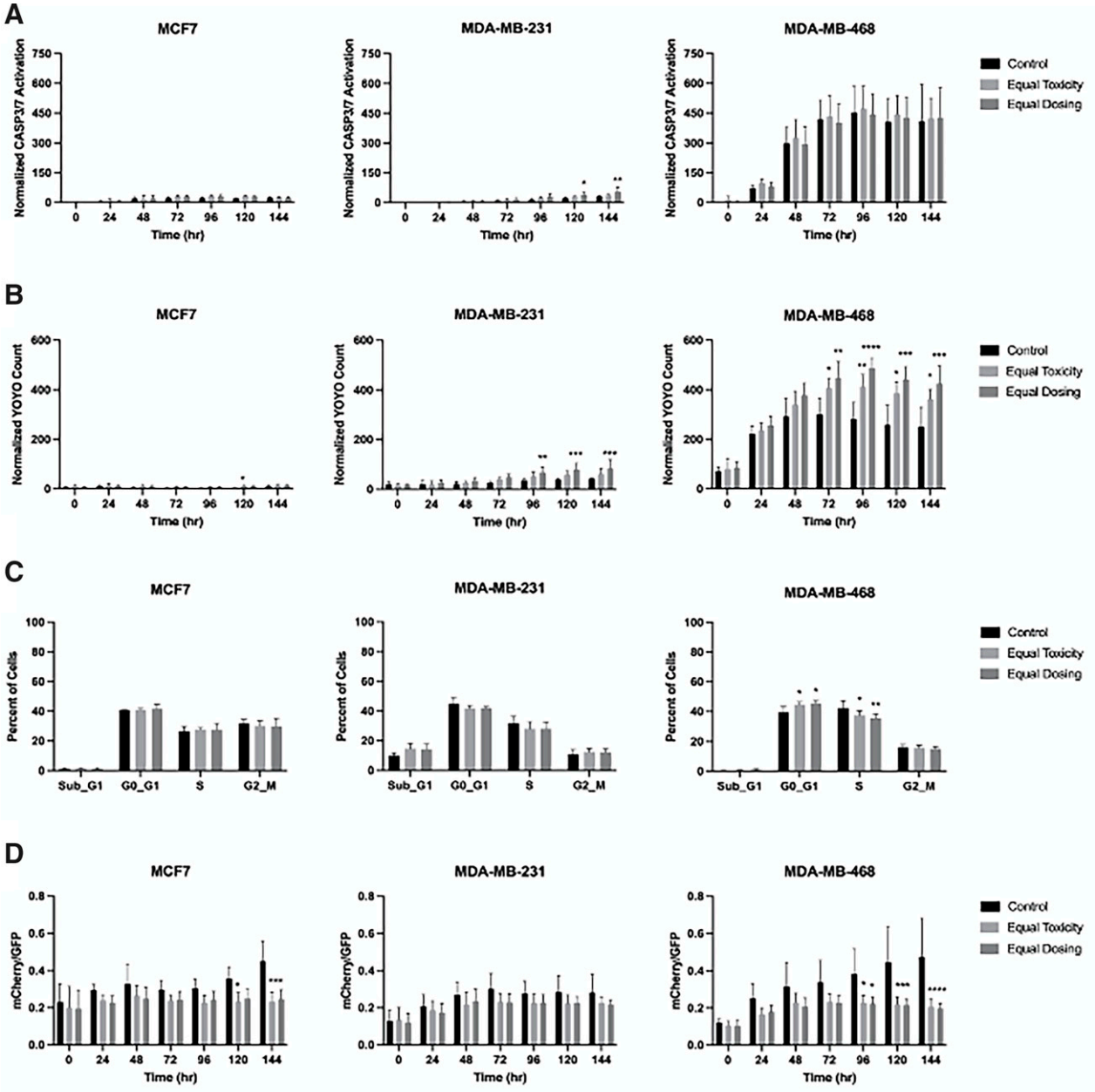

Fig. 3. Cell death, cell cycle, and autophagic flux after HCQ treatment in tumor organoids. (A) Cell death via caspase 3/7 staining in the IncuCyte. Green object integrated intensity was normalized to red object integrated intensity. (B) Cell death analysis by YOYO staining in the IncuCyte. Green object integrated intensity was normalized to red object integrated intensity. (C) Cell cycle analysis via EdU incorporation. (D) Autophagy inhibition assessed by monitoring LC3-mCherry-GFP–labeled cells in the IncuCyte over 6 days. $N = 3$ or more biologic replicates of three technical replicates each. Significance indicated is compared with control. *$P \leq 0.05$, **$P \leq 0.01$, ***$P \leq 0.001$, and ****$P \leq 0.0001$.

7C). MCF7 and MDA-MB-468 organoid autophagic flux inhibition was sustained and enhanced by 144 hours. MDA-MB-231 organoid autophagic flux inhibition after HCQ was less marked compared with control, which was consistent with the 2D cell culture results.

Autophagy–Dependent Tumors Take Up More HCQ In Vivo. To assess how HCQ affects autophagy-dependent and -independent tumors in vivo, MCF7, MDA-MB-231, or MDA-MB-468 cells were implanted into mice, and once the tumors were at least 100 mm^3, the mice were treated with either 60 mg/kg HCQ once or daily for 1 week to analyze steady-state levels.

Whole-blood HCQ and DHCQ amounts were similar in both MDA-MB-231 and MCF7 cohorts, whereas both tumor HCQ and DHCQ amounts were higher in MDA-MB-231 compared with MCF7 after single HCQ doses. MDA-MB-468 HCQ and DHCQ amounts were also similar to MDA-MB-231 (Fig. 4A). Tumor levels of HCQ and DHCQ were higher in MDA-MB-231 and MDA-MB-468 compared with MCF7 at steady state (Fig. 4B), indicating that more HCQ and DHCQ are distributed into autophagy-sensitive tumors. In the steady-state cohort, whole-blood levels were similar for HCQ and DHCQ in MDA-MB-231 and MCF7 but the MDA-MB-231 cohort had higher tumor HCQ and DHCQ levels compared with the

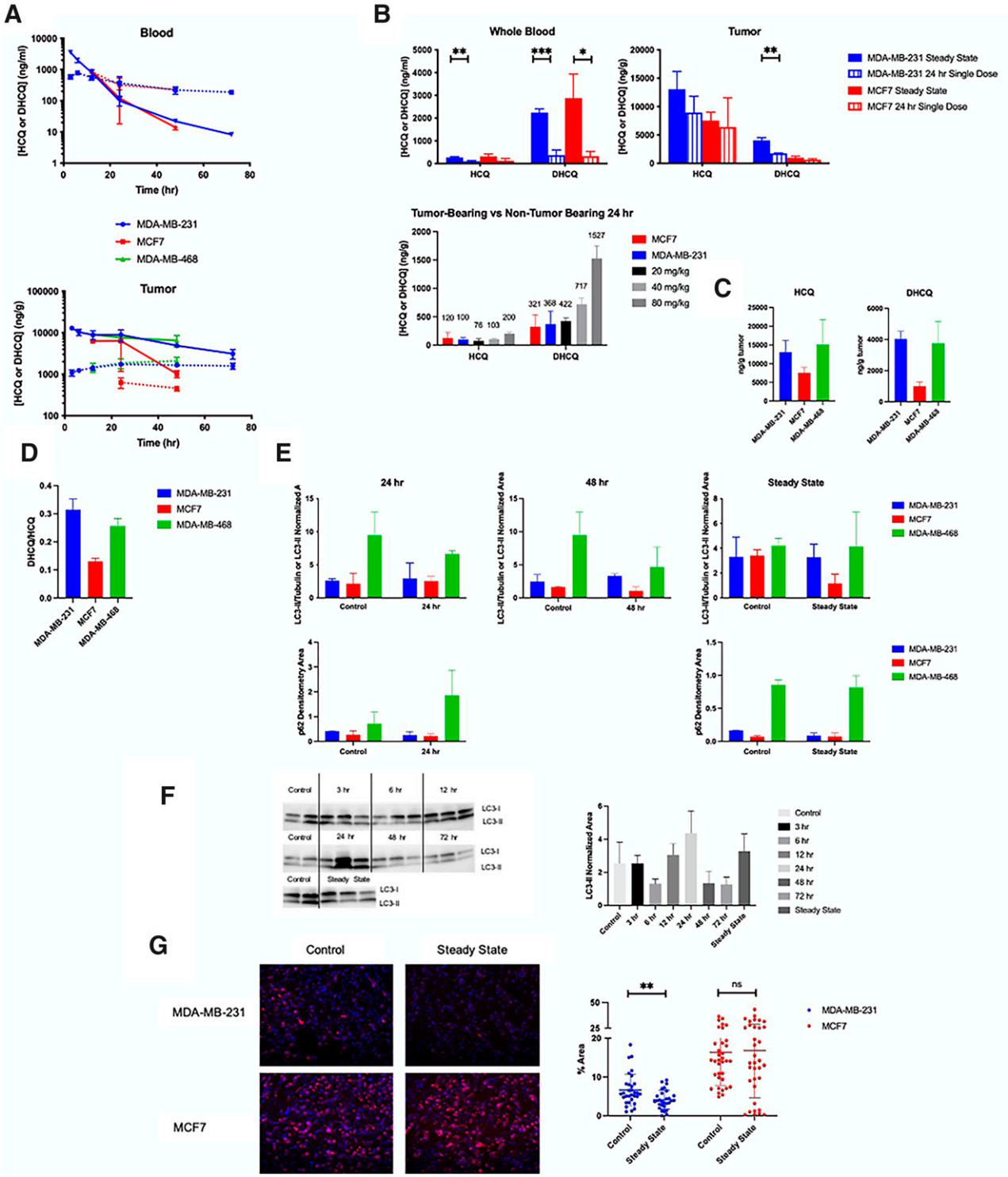

Fig. 4. HCQ PK and PD in breast tumor–bearing mice. (A) Exposure of HCQ and DHCQ in whole blood and tumor. Solid lines represent HCQ, and dotted lines represent DHCQ. (B) Blood and tumor HCQ and DHCQ amounts detected in steady-state–dosed mice compared with 24-hour single-dose mice (top) and HCQ and DHCQ amounts detected in blood in single-dose 24-hour tumor-bearing mice compared with non–tumor-bearing mice at 24 hours (bottom). Numbers listed above the bars are the mean amount of HCQ/DHCQ of the respective cohort. (C) Tumor levels of HCQ and DHCQ at steady state. (D) DHCQ:HCQ ratios in tumors. (E) Western blot quantification of LC3-II/tubulin, LC3-II densitometry area normalized by total protein, or p62 densitometry area normalized by total protein in breast tumors after 24 hours, 48 hours, or steady-state dosing of HCQ in mice. Western blots used for protein quantification in Supplemental Fig. 5. (F) Western blot and quantification of LC3-II density normalized to total protein over 72 hours or at steady state. (G) Immunofluorescent analysis of Ki67 in MDA-MB-231 and MCF7 control and steady-state tumors. Blue = 4′,6-diamidino-2-phenylindole, and red = Ki67. Quantification based on six or more separate fields of view on each tumor slice. $N = 3$ mice per group. *$P \leq 0.05$, **$P \leq 0.01$, ***$P \leq 0.001$, and ****$P \leq 0.0001$.

MCF7 cohort (Fig. 4C). When the steady-state tumor group was compared with the 24-hour single-dose tumors in each tumor type, HCQ and DHCQ levels were significantly higher in tumors in the steady-state group compared with the single-dose groups (Fig. 4C), indicating that HCQ and DHCQ move into the tumor after 24 hours and tumor and blood saturation is not achieved by 24 hours. Whole blood of tumor-bearing mice treated with a single dose of HCQ for 24 hours was compared with the non–tumor-bearing mice treated with HCQ for 24 hours from Fig. 1. HCQ levels from the tumor-bearing mice fell between the 40 and 80 mg/kg non–tumor-bearing levels as expected (Fig. 4C), and PK parameters fell within the expected range (Table 1). DHCQ levels were not as high in whole blood in tumor-bearing mice compared with levels that would be predicted based on the non–tumor-bearing mice, but this could be because of DHCQ sequestering in tumors in the tumor-bearing mice. When analyzing DHCQ:HCQ ratios found in steady-state treated tumors, MDA-MB-231 and MDA-MB-468 had higher ratios compared with MCF7 (Fig. 4D), indicating that more DHCQ was formed compared with HCQ in the autophagy-dependent tumors.

Autophagic Responses Were Not Different, but Proliferation Was Less in Autophagy-Dependent Tumors In Vivo. Pharmacodynamic response was evaluated via Western blot analysis of LC3 and p62 in the MDA-MB-231, MCF7, and MDA-MB-468 cohorts. There were no major differences between control and treated mice at 24 hours, 48 hours, or steady-state doses, although p62 levels trended higher in treated MDA-MB-468 tumors at 24 hours (Fig. 4E; Supplemental Fig. 5). LC3-II densitometry areas normalized to total protein were highest at 12 hours, 24 hours, and after steady-state dosing in MDA-MB-231 tumors, but these results were variable depending on the mouse (Fig. 4F). Tumor cell proliferation was measured via immunofluorescence staining of Ki67 in the MDA-MB-231 and MCF7 control and steady-state cohorts. MDA-MB-231 tumors had significantly less Ki67 staining after HCQ treatment, whereas there was no difference in cell proliferation in the MCF7 tumors after HCQ treatment (Fig. 4G). These results are consistent with the cell cycle results in 2D culture (Fig. 2D) and tumor organoids (Fig. 3C) because the cells that are more sensitive to autophagy inhibition (MDA-MB-231 and MDA-MB-468) have fewer proliferative cells at lower HCQ concentrations compared with those that are not (MCF7). Apoptotic cell death via immunofluorescence staining of cleaved caspase-3 was also performed, but no tumors expressed cleaved caspase-3 (unpublished data).

Discussion

Autophagy, a lysosomal degradation process that recycles cellular components, has been linked to enhanced cancer cell survival and chemotherapy resistance. HCQ is repurposed as an anticancer agent that inhibits autophagy. Although it is currently being used in over 90 cancer clinical trials alone or in combination treatments, pharmacodynamic responses associated with drug dosages used clinically are unclear. Further, preclinical studies in mice use varying doses of HCQ, but there is no rationale behind those doses or the effect the associated drug exposures have on autophagy inhibition in vivo.

This study showed that HCQ and its major active metabolite DHCQ levels are dose-dependent in whole blood and multiple tissues in vivo (Fig. 1A; Supplemental Fig. 1). Autophagy inhibition was achieved at all doses in the liver and gut at multiple time points (Fig. 1C). Although some autophagy inhibition was observed at various doses in multiple tissues, there was high variability between different mice. Variability and nonsignificant differences in autophagy inhibition are also evident in the clinic (Barnard et al., 2014; Mahalingam et al., 2014; Wolpin et al., 2014), and the results here show that this is difficult to control from patient to patient based on dose alone, which suggests HCQ doses may need to be tailored based on their individual PD response. It further implies that autophagy inhibition may not be reliably achievable using HCQ and that more potent autophagy inhibitors, such as DC661, should be considered. This work clarified that 60 ± 20 mg/kg HCQ is the HED to give mice in preclinical studies and validates the clinical relevance for studies that choose HCQ doses within this range (Fig. 1B). Calculating the HED in this way highlights the importance of normalizing preclinical and clinical drug exposure because mouse model efficacy is predictive of clinical response when drug concentrations in mice are appropriately corrected for therapeutic exposure (Kerbel, 2003; Wong et al., 2012).

Mice with breast tumors treated with the HED of 60 mg/kg HCQ had similar whole-blood HCQ and DHCQ levels but varying tumor levels with more detected in the autophagy-dependent MDA-MB-231 and MDA-MB-468 tumors compared with autophagy-independent MCF7 tumors (Maycotte et al., 2014) (Fig. 4A), which suggests that autophagy-dependent tumors sequester more HCQ over time. This could be because of an increase in lysosomes in autophagy-dependent tumors compared with autophagy-independent tumors (Collins et al., 2021). There are important implications of this when considering dual treatment with HCQ and other drugs, especially chemotherapies that sequester in lysosomes. It could be advantageous to treat patients with HCQ prior to these drugs since HCQ also sequesters in lysosomes and could make these drugs more potent, as seen in a phase I clinical trial in dogs with lymphoma (Barnard et al., 2014). Although much information exists on HCQ effects in cancer, it is also important to consider DHCQ since it is present at relevant concentrations and correlates to liver autophagy inhibition (Fig. 1D; Supplemental Fig. 3). Further, data here suggest that DHCQ:HCQ ratios may be predictive of patient efficacy based on autophagy dependence of the tumor; this ratio has been implicated in patient response to HCQ treatment in other studies (Munster et al., 2002; Lee et al., 2016). Similar to HCQ, DHCQ has a long half-life of approximately 160 hours in people (Munster et al., 2002). However, DHCQ is not produced in cell culture experiments because there are no cytochrome P450 enzymes. Since in vitro studies do not take into account DHCQ, but it has the same action as HCQ, drug concentrations used in vitro likely do not reflect the full efficacy HCQ and subsequent DHCQ will have on PD, and this should be taken into consideration when choosing HCQ doses in vitro. This is evidenced by comparing HCQ exposure in vitro to in vivo exposure, wherein 20 μM HCQ dosing in cell culture correlates best with the autophagy-dependent tumors, whereas there is no correlation between MCF7 and in vitro exposure (Fig. 5). Furthermore, adding in relevant DHCQ exposure means that a higher concentration of HCQ can be used in cell culture to achieve the same exposure observed in vivo (Fig. 5). This also highlights the importance of calculating maximum achievable clinically relevant doses for cell culture experiments.

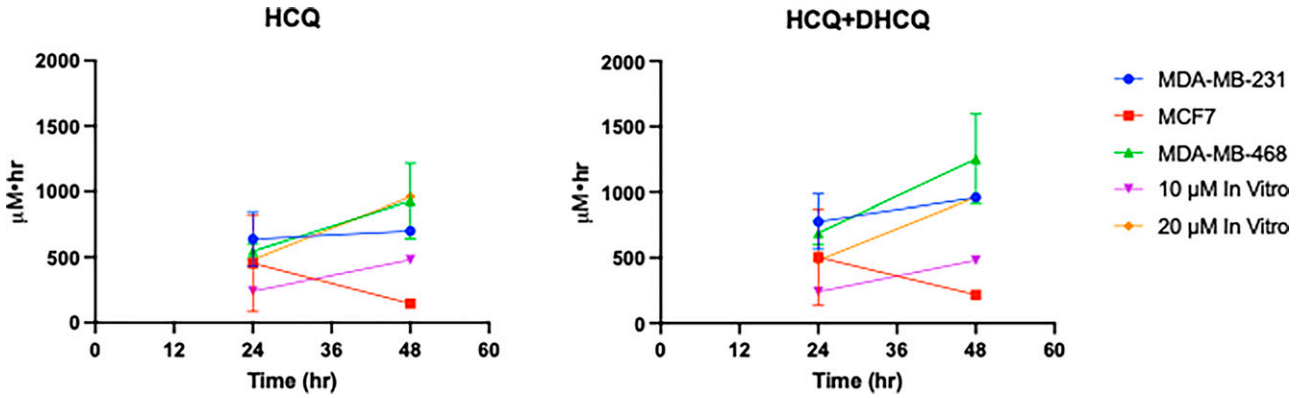

Fig. 5. HCQ PK exposure in vitro compared with in vivo at 24 and 48 hours. For the breast tumors, exposure is based on AUC of concentration vs. time curves. The 10 and 20 μM in vitro AUC is based on the theoretical exposure cells will experience based on those doses for the given time (e.g., 10 μM × 24 hours = 240 hours × μM).

Autophagy inhibition measured by Western blot in vivo was less conclusive in all tumor types, which is consistent with the non–tumor-bearing data and autophagy inhibition measured clinically. However, autophagy inhibition was observed in vitro at clinically relevant concentrations. Inhibition was most enhanced at later time points, indicating that HCQ does not decrease autophagic flux rapidly (Figs. 2E and 3D) even though HCQ uptake is observed at early time points in the tumors. This is consistent with observing decreased cell growth compared with control after HCQ treatment at later time points (Fig. 2A). Furthermore, MDA-MB-231 showed high basal autophagy even when treated with HCQ, implying that HCQ is inhibiting autophagy but not as well as other autophagy inhibitors since this assay was based on autophagy inhibition via bafilomycin A1. Both autophagy-dependent and -independent cell lines had significant decreases in autophagic flux, indicating autophagy is still inhibited by HCQ irrespective of autophagy dependence. In contrast, one study found the basal breast cancer line SUM190 to be the most sensitive to HCQ-induced autophagy inhibition in vitro, but that could be because it only analyzed short time points (Wang et al., 2019a). Overall, autophagy inhibition was variable in vivo but observed in vitro, suggesting that other autophagy PD measures may be necessary to better understand how HCQ is causing autophagy inhibition in vivo and clinically.

Although autophagy inhibition was inconsistent across tumor types and between controlled and treated mice, cell proliferation was consistently affected in autophagy-sensitive MDA-MB-231 and MDA-MB-468 tumors treated with HCQ but not in autophagy-independent MCF7 tumors (Figs. 2D, 3C, and 4G), which indicates that autophagy-dependent tumors are more affected by single-agent HCQ. Furthermore, cell proliferation was more affected in autophagy-dependent tumors at lower doses of HCQ compared with MCF7 (Figs. 2D and 3C), suggesting that the MCF7 tumors in vivo did not have high enough HCQ levels to cause decreased cell proliferation that was observed in MDA-MB-231. The ability of HCQ alone to inhibit cell proliferation varies in tumor types (Xie et al., 2013; Arnaout et al., 2019), suggesting that chloroquine and HCQ alone may not provide effective antiproliferative effects in many patients with cancer but that HCQ alone is antiproliferative if tumors are inherently dependent on autophagy. Even though HCQ did decrease cell proliferation in autophagy-dependent tumors, more potent autophagy inhibitors may produce more robust results and have less variability in achieving autophagy inhibition as a single agent compared with HCQ.

Clinically relevant HCQ concentrations were used in this study to determine whether HCQ causes cancer cell death. Based on in vivo and in vitro apoptosis and cell death assays, breast cancer treated with HCQ alone at the concentrations used here do not appear to die via caspase 3/7–dependent apoptosis but do undergo some cell death in 2D and organoids (Fig. 3B; Supplemental Fig. S4A), and this cell death is enhanced in autophagy-dependent tumors at later time points. Another study also observed no caspase-3–dependent cell death in head and neck squamous cell carcinoma after 20 μM HCQ alone (Gao et al., 2018). Other studies have shown that HCQ alone can induce caspase-3–dependent cell death in gastric (Wang et al., 2019b) a nd bladder cancer (Lin et al., 2017) at HCQ concentrations of 14 and 20 μM, respectively, indicating that HCQ alone will only induce this kind of cell death at clinically achievable concentrations in certain cancer types. However, when clinically relevant HCQ doses are combined with other treatments, HCQ enhances apoptotic cell death in other cancer types, such as head and neck squamous cell carcinoma (Gao et al., 2018), melanoma (Xie et al., 2013), and gastric cancer (Wang et al., 2019b), demonstrating that although low enough doses of HCQ alone do not cause caspase 3/7–dependent apoptosis in certain cancer types, in combination with other therapies it does induce caspase 3/7–dependent apoptosis. Combination therapies were not tested in this study, but the results here and in other studies suggest that combining HCQ with other treatments may enhance cell death in breast cancer.

Overall, this study shows that 2D cell culture, three-dimensional tumor organoids, and in vivo studies produce similar results, and in vitro studies can be used as surrogates to recapitulate in vivo tumor responses. Tumor autophagy dependence is important in the evocation of cellular responses including autophagy inhibition, cell proliferation, and cell death. Furthermore, in certain contexts, HCQ may not be an adequate drug as a single agent depending on the clinical objective. DHCQ is an active metabolite whose effects need to be considered in in vitro experiments since it is not produced but would add to toxicity if it were present. Lastly, better

biomarkers to measure autophagy inhibition clinically are necessary to understand how the PD relates to the PK of autophagy inhibitors.

Authorship Contributions

Participated in research design: Van Eaton, Gustafson.

Conducted experiments: Van Eaton.

Performed data analysis: Van Eaton, Gustafson.

Wrote or contributed to the writing of the manuscript: Van Eaton, Gustafson.

Acknowledgments

The authors would like to thank Drs. Ryan Hansen and Keagan Collins for contributions in the pharmacokinetic studies as well as other staff in the Pharmacology Shared Resource.

References

Amaravadi RK, Lippincott-Schwartz J, Yin XM, Weiss WA, Takebe N, Timmer W, DiPaola RS, Lotze MT, and White E (2011) Principles and current strategies for targeting autophagy for cancer treatment. *Clin Cancer Res* **17**:654–666.

Amaravadi RK, Yu D, Lum JJ, Bui T, Christophorou MA, Evan GI, Thomas-Tikhonenko A, and Thompson CB (2007) Autophagy inhibition enhances therapy-induced apoptosis in a Myc-induced model of lymphoma. *J Clin Invest* **117**:326–336.

Arnaout A, Robertson SJ, Pond GR, Lee H, Jeong A, Ianni L, Kroeger L, Hilton J, Coupland S, Gottlieb C, et al. (2019) A randomized, double-blind, window of opportunity trial evaluating the effects of chloroquine in breast cancer patients. *Breast Cancer Res Treat* **178**:327–335.

Barnard RA, Wittenburg LA, Amaravadi RK, Gustafson DL, Thorburn A, and Thamm DH (2014) Phase I clinical trial and pharmacodynamic evaluation of combination hydroxychloroquine and doxorubicin treatment in pet dogs treated for spontaneously occurring lymphoma. *Autophagy* **10**:1415–1425.

Bleijs M, van de Wetering M, Clevers H, and Drost J (2019) Xenograft and organoid model systems in cancer research. *EMBO J* **38**:e101654.

Boehrer S, Adès L, Braun T, Galluzzi L, Grosjean J, Fabre C, Le Roux G, Gardin C, Martin A, de Botton S, et al. (2008) Erlotinib exhibits antineoplastic off-target effects in AML and MDS: a preclinical study. *Blood* **111**:2170–2180.

Campaner E, Zannini A, Santorsola M, Bonazza D, Bottin C, Cancila V, Tripodo C, Bortul M, Zanconati F, Schoeftner S, et al. (2020) Breast cancer organoids model patient-specific response to drug treatment. *Cancers (Basel)* **12**:3869.

Cardoso CD and Bonato PS (2009) Enantioselective metabolism of hydroxychloroquine employing rats and mice hepatic microsomes. *Braz J Pharm Sci* **45**:659–667.

Carmichael SJ, Charles B, and Tett SE (2003) Population pharmacokinetics of hydroxychloroquine in patients with rheumatoid arthritis. *Ther Drug Monit* **25**:671–681.

Cheong H (2015) Integrating autophagy and metabolism in cancer. *Arch Pharm Res* **38**:358–371.

Collins KP, Witta S, Coy JW, Pang Y, and Gustafson DL (2021) Lysosomal biogenesis and implications for hydroxychloroquine disposition. *J Pharmacol Exp Ther* **376**:294–305.

De Duve C and Wattiaux R (1966) Functions of lysosomes. *Annu Rev Physiol* **28**:435–492.

Dobrolecki LE, Airhart SD, Alferez DG, Aparicio S, Behbod F, Bentires-Alj M, Brisken C, Bult CJ, Cai S, Clarke RB, et al. (2016) Patient-derived xenograft (PDX) models in basic and translational breast cancer research. *Cancer Metastasis Rev* **35**:547–573.

Ducharme J and Farinotti R (1996) Clinical pharmacokinetics and metabolism of chloroquine. Focus on recent advancements. *Clin Pharmacokinet* **31**:257–274.

Duffy A, Le J, Sausville E, and Emadi A (2015) Autophagy modulation: a target for cancer treatment development. *Cancer Chemother Pharmacol* **75**:439–447.

Duran A, Linares JF, Galvez AS, Wikenheiser K, Flores JM, Diaz-Meco MT, and Moscat J (2008) The signaling adaptor p62 is an important NF-kappaB mediator in tumorigenesis. *Cancer Cell* **13**:343–354.

Estes ML, Ewing-Wilson D, Chou SM, Mitsumoto H, Hanson M, Shirey E, and Ratliff NB (1987) Chloroquine neuromyotoxicity. Clinical and pathologic perspective. *Am J Med* **82**:447–455.

Fan H, Demirci U, and Chen P (2019) Emerging organoid models: leaping forward in cancer research. *J Hematol Oncol* **12**:142.

Frese KK and Tuveson DA (2007) Maximizing mouse cancer models. *Nat Rev Cancer* **7**:645–658.

Furst DE (1996) Pharmacokinetics of hydroxychloroquine and chloroquine during treatment of rheumatic diseases. *Lupus* **5** (Suppl 1):S11–S15.

Gao L, Zhao X, Lang L, Shay C, Andrew Yeudall W, and Teng Y (2018) Autophagy blockade sensitizes human head and neck squamous cell carcinoma towards CYT997 through enhancing excessively high reactive oxygen species-induced apoptosis. *J Mol Med (Berl)* **96**:929–938.

Goldberg SB, Supko JG, Neal JW, Muzikansky A, Digumarthy S, Fidias P, Temel JS, Heist RS, Shaw AT, McCarthy PO, et al. (2012) A phase I study of erlotinib and hydroxychloroquine in advanced non-small-cell lung cancer. *J Thorac Oncol* **7**:1602–1608.

Kerbel RS (2003) Human tumor xenografts as predictive preclinical models for anticancer drug activity in humans: better than commonly perceived-but they can be improved. *Cancer Biol Ther* **2**(4, Suppl 1)S134–S139.

Kimmelman AC (2011) The dynamic nature of autophagy in cancer. *Genes Dev* **25**:1999–2010.

Komatsu M, Waguri S, Koike M, Sou YS, Ueno T, Hara T, Mizushima N, Iwata J, Ezaki J, Murata S, et al. (2007) Homeostatic levels of p62 control cytoplasmic inclusion body formation in autophagy-deficient mice. *Cell* **131**:1149–1163.

Lee JY, Vinayagamoorthy N, Han K, Kwok SK, Ju JH, Park KS, Jung SH, Park SW, Chung YJ, and Park SH (2016) Association of polymorphisms of cytochrome P450 2D6 with blood hydroxychloroquine levels in patients with systemic lupus erythematosus. *Arthritis Rheumatol* **68**:184–190.

Li X, Pan B, Ma J, Zhao Z, and Li M (2019) Breast cancer organoids model treatment response of Her2 targeted therapy in her2-mutant breast cancer. *Ann Oncol* **30**:v768–v769.

Lim HS, Im JS, Cho JY, Bae KS, Klein TA, Yeom JS, Kim TS, Choi JS, Jang IJ, and Park JW (2009) Pharmacokinetics of hydroxychloroquine and its clinical implications in chemoprophylaxis against malaria caused by Plasmodium vivax. *Antimicrob Agents Chemother* **53**:1468–1475.

Lin YC, Lin JF, Wen SI, Yang SC, Tsai TF, Chen HE, Chou KY, and Hwang TI (2017) Chloroquine and hydroxychloroquine inhibit bladder cancer cell growth by targeting basal autophagy and enhancing apoptosis. *Kaohsiung J Med Sci* **33**:215–223.

Mahalingam D, Mita M, Sarantopoulos J, Wood L, Amaravadi RK, Davis LE, Mita AC, Curiel TJ, Espitia CM, Nawrocki ST, et al. (2014) Combined autophagy and HDAC inhibition: a phase I safety, tolerability, pharmacokinetic, and pharmacodynamic analysis of hydroxychloroquine in combination with the HDAC inhibitor vorinostat in patients with advanced solid tumors. *Autophagy* **10**:1403–1414.

Manic G, Obrist F, Kroemer G, Vitale I, and Galluzzi L (2014) Chloroquine and hydroxychloroquine for cancer therapy. *Mol Cell Oncol* **1**:e29911.

Mauthe M, Orhon I, Rocchi C, Zhou X, Luhr M, Hijlkema KJ, Coppes RP, Engedal N, Mari M, and Reggiori F (2018) Chloroquine inhibits autophagic flux by decreasing autophagosome-lysosome fusion. *Autophagy* **14**:1435–1455.

Maycotte P, Gearheart CM, Barnard R, Aryal S, Mulcahy Levy JM, Fosmire SP, Hansen RJ, Morgan MJ, Porter CC, Gustafson DL, et al. (2014) STAT3-mediated autophagy dependence identifies subtypes of breast cancer where autophagy inhibition can be efficacious. *Cancer Res* **74**:2579–2590.

Munster T, Gibbs JP, Shen D, Baethge BA, Botstein GR, Caldwell J, Dietz F, Ettlinger R, Golden HE, Lindsley H, et al. (2002) Hydroxychloroquine concentration-response relationships in patients with rheumatoid arthritis. *Arthritis Rheum* **46**:1460–1469.

Rosenfeld MR, Ye X, Supko JG, Desideri S, Grossman SA, Brem S, Mikkelson T, Wang D, Chang YC, Hu J, et al. (2014) A phase I/II trial of hydroxychloroquine in conjunction with radiation therapy and concurrent and adjuvant temozolomide in patients with newly diagnosed glioblastoma multiforme. *Autophagy* **10**:1359–1368.

Ruiz-Irastorza G, Ramos-Casals M, Brito-Zeron P, and Khamashta MA (2010) Clinical efficacy and side effects of antimalarials in systemic lupus erythematosus: a systematic review. *Ann Rheum Dis* **69**:20–28.

Sasmita AO and Wong YP (2018) Organoids as reliable breast cancer study models: An update. *Int J Oncol Res* **1**:008.

Sflomos G, Dormoy V, Metsalu T, Jeitziner R, Battista L, Scabia V, Raffoul W, Delaloye JF, Treboux A, Fiche M, et al. (2016) A preclinical model for ERalpha-positive breast cancer points to the epithelial microenvironment as determinant of luminal phenotype and hormone response. *Cancer Cell* **29**:407–422.

Tett SE (1993) Clinical pharmacokinetics of slow-acting antirheumatic drugs. *Clin Pharmacokinet* **25**:392–407.

Thorburn A, Thamm DH, and Gustafson DL (2014) Autophagy and cancer therapy. *Mol Pharmacol* **85**:830–838.

Wang P, Du Y, and Wang J (2019a) Indentification of breast cancer subtypes sensitive to HCQ-induced autophagy inhibition. *Pathol Res Pract* **215**:152609.

Wang W, Liu L, Zhou Y, Ye Q, Yang X, Jiang J, Ye Z, Gao F, Tan X, Zhang G, et al. (2019b) Hydroxychloroquine enhances the antitumor effects of BC001 in gastric cancer. *Int J Oncol* **55**:405–414.

Wolpin BM, Rubinson DA, Wang X, Chan JA, Cleary JM, Enzinger PC, Fuchs CS, McCleary NJ, Meyerhardt JA, Ng K, et al. (2014) Phase II and pharmacodynamic study of autophagy inhibition using hydroxychloroquine in patients with metastatic pancreatic adenocarcinoma. *Oncologist* **19**:637–638.

Wong H, Choo EF, Alicke B, Ding X, La H, McNamara E, Theil FP, Tibbitts J, Friedman LS, Hop CE, et al. (2012) Antitumor activity of targeted and cytotoxic agents in murine subcutaneous tumor models correlates with clinical response. *Clin Cancer Res* **18**:3846–3855.

Xie X, White EP, and Mehnert JM (2013) Coordinate autophagy and mTOR pathway inhibition enhances cell death in melanoma. *PLoS One* **8**:e55096.

Yang L, Liu B, Chen H, Gao R, Huang K, Guo Q, Li F, Chen W, and He J (2020) Progress in the application of organoids to breast cancer research. *J Cell Mol Med* **24**:5420–5427.

Yang S, Wang X, Contino G, Liesa M, Sahin E, Ying H, Bause A, Li Y, Stommel JM, Dell'antonio G, et al. (2011) Pancreatic cancers require autophagy for tumor growth. *Genes Dev* **25**:717–729.

Yang Z and Klionsky DJ (2010) Eaten alive: a history of macroautophagy. *Nat Cell Biol* **12**:814–822.

Zeh HJ, Bahary N, Boone BA, Singhi AD, Miller-Ocuin JL, Normolle DP, Zureikat AH, Hogg ME, Bartlett DL, Lee KK, et al. (2020) A randomized Phase II preoperative study of autophagy inhibition with high-dose hydroxychloroquine and gemcitabine/nab-paclitaxel in pancreatic cancer patients. *Clin Cancer Res* **26**:3126–3134.

Address correspondence to: Dr. Daniel L. Gustafson, Flint Animal Cancer Center, 300 W. Drake Rd, Fort Collins, CO 80523. Email: Daniel.Gustafson@colostate.edu